axioms

MDPI

Article

On the Combination of the Laplace Transform and Integral Equation Method to Solve the 3D Parabolic Initial Boundary Value Problem

Roman Chapko * and Svyatoslav Lavryk

Department of Computational Mathematics, Ivan Franko National University of Lviv, Universytetska Str. 1, 79000 Lviv, Ukraine; sviatoslav.lavryk@lnu.edu.ua
* Correspondence: roman.chapko@lnu.edu.ua

Abstract

We consider a two-step numerical approach for solving parabolic initial boundary value problems in 3D simply connected smooth regions. The method uses the Laplace transform in time, reducing the problem to a set of independent stationary boundary value problems for the Helmholtz equation with complex parameters. The inverse Laplace transform is computed using a sinc quadrature along a suitably chosen contour in the complex plane. We show that due to a symmetry of the quadrature nodes, the number of stationary problems can be decreased by almost a factor of two. The influence of the integration contour parameters on the approximation error is also researched. Stationary problems are numerically solved using a boundary integral equation approach applying the Nyström method, based on the quadratures for smooth surface integrals. Numerical experiments support the expectations.

Keywords: heat equation; Helmholtz equation; 3D initial boundary value problem; numerical Laplace transform inversion; boundary integral equation method; Nyström method; Wienert quadratures; sinc quadratures

MSC: 35J05; 35K05; 35K20; 44A10; 45B05; 65D32; 65R10; 65R20

Academic Editors: Gradimir V. Milovanović, Pengzhan Huang and Yinnian He

Received: 30 July 2025
Revised: 27 August 2025
Accepted: 28 August 2025
Published: 29 August 2025

Citation: Chapko, R.; Lavryk, S. On the Combination of the Laplace Transform and Integral Equation Method to Solve the 3D Parabolic Initial Boundary Value Problem. *Axioms* **2025**, *14*, 666. https://doi.org/10.3390/axioms14090666

1. Introduction

The boundary integral equation (BIE) method is a very powerful approach for the numerical solution of various boundary value problems (BVPs). The main advantage of the BIE method consists in the dimensionality decrease of the given differential problem: the BVP is reduced to the BIE, where the unknown function is defined only on the domain boundary [1]. Clearly, the considered differential equation needs to have a fundamental solution and be homogeneous. For the numerical solution of such a BIE, effective numerical methods have been developed, for example, projection methods [1].

In the case of non-stationary BVPs, there are additional difficulties caused by the presence of time as an independent variable. There are several ways to apply the BIE to such BVPs [2]. One approach involves a fundamental solution of the time-dependent differential equation. Then, by a direct or indirect BIE method, the initial BVP can be reduced to a time-domain boundary integral equation. The numerical solution of such a BIE is more difficult than in the stationary case. The most popular method for time-domain boundary integral equations is the convolution quadrature method suggested by Christian Lubich in the 1980s [3].

Another so-called two-step method consists of the semi-discretization of the given initial BVP with respect to the time variable. As a result, the set of stationary BVPs for elliptic equations is obtained. This time discretization can be achieved using approaches such as finite-difference approximations (e.g., the Rothe method [4]) or integral transforms (e.g., the Laguerre transform [5,6], the Laplace transform [7]). In the second step, which addresses the spatial variable, various techniques are available, including the BIE method. Two-step methods offer several advantages, such as dimension reduction and the avoidance of volume integrals. The finite-difference semi-discretization is the simplest approach, which gives the numerical solution in a fixed set of time moments. In the case of integral transforms, we have an approximation for an arbitrary time, but it is necessary to calculate the inverse transform numerically.

The application of the Laplace transform to time-dependent problems has a long history. It can be used in combination with the finite difference method [8], finite element method [9], boundary element method [10,11] and others. In the case of the parabolic initial BVP, stationary BVPs for the Helmholtz-type equations with complex parameters can be obtained. The inverse Laplace transform is defined as the Bromwich integral on the complex plane, and there are multiple numerical methods for its calculation (see [7,12–19] and references therein).

In this paper, we use the two-step approach based on the Laplace transform and the BIE method to solve parabolic initial BVPs in 3D domains. To calculate the inverse transform, the sinc-quadrature rule suggested in [13] is applied. This leads to a set of independent BVPs for the Helmholtz-type equation, which can be numerically solved in parallel. We consider the case of specific smooth surfaces, diffeomorphic to the unit sphere. It provides the possibility of applying effective numerical schemes for the received BIE. We apply the Nyström method based on the Wienert's quadrature rules for the surface integrals [20].

The main contribution of this work is reducing computational costs by selecting optimal values for the inverse Laplace transform's contour parameters, decreasing the number of stationary BVPs due to the symmetry of the quadrature nodes and applying an efficient method for numerically solving the resulting BIEs.

The outline of the present work is as follows. In Section 2, we apply the Laplace transform to the parabolic initial boundary value problem and describe the sinc quadrature for the numerical inverse transform. Two ideas for decreasing computational cost are presented in Sections 2.1 and 2.2. In Section 2.1, it is shown that due to a certain symmetry of the sinc-quadrature nodes, the number of stationary problems can be reduced almost twice. In Section 2.2 reflects how the choice of integration contour in the complex plane influences the precision of the sinc quadrature. In Section 3, we apply the indirect BIE method to stationary elliptic problems. The unknown solution is presented in the form of a double-layer potential, and a BIE of the second kind is obtained. Taking into account that the boundary surface is diffeomorphic to the unit sphere, we apply the Nyström method based on the Wienert's quadrature rules. Section 4 presents numerical examples to clarify our approach and its optimization.

Before closing this section, we formulate the problem to be studied. Let $D \subset \mathbb{R}^3$ be a simply connected region with a smooth boundary Γ. It is necessary to find function $u \in C^{2,1}(D \times (0,\infty)) \cap C(\overline{D} \times [0,\infty))$, which satisfies the heat equation

$$\frac{\partial u}{\partial t}(x,t) = \Delta u(x,t), \quad (x,t) \in D \times (0,\infty), \tag{1}$$

the initial condition

$$u(x,0) = 0, \quad x \in D \tag{2}$$

and the Dirichlet boundary value condition

$$u(x,t) = g(x,t), \quad (x,t) \in \Gamma \times (0,\infty). \tag{3}$$

Assume that the given function g is bounded and continuous and satisfies the compatibility condition $g(x,0) = 0, \quad x \in \Gamma$.

We consider surfaces Γ, diffeomorphic to the unit sphere

$$\mathbb{S}^2 = \{p(\theta,\phi) = (\sin\theta\cos\phi, \sin\theta\sin\phi, \cos\theta),\ (\theta,\phi) \in [0,\pi] \times [0,2\pi)\}$$

described by an analytic function $q : \mathbb{S}^2 \to \Gamma$ with a nonzero Jacobian J.

2. Time Semi-Discretization via Laplace Transform

The Laplace transform of a function $f(t)$ is given by

$$\mathcal{L}_t(f) = F(s) = \int_0^\infty e^{-st} f(t)dt, \quad s = \sigma + i\tau,\ s \in \mathbb{C}. \tag{4}$$

The integral in (4) is convergent for $\mathrm{Re}(s) > a_0$, where a_0 is the order of growth of function $f(t)$, and $F(s)$ is an analytic function [21].

For the known image F, the original f can be reconstructed by using the inverse Laplace transform, described by the Bromwich integral

$$\mathcal{L}_s^{-1}(F) = f(t) = \frac{1}{2\pi i}\int_C e^{st}F(s)ds, \tag{5}$$

where C is a suitable integration contour (see [7,13–16] and references therein).

A popular strategy to use the Laplace transform for the heat problems is as follows:

1. Apply the Laplace transform in time to the initial boundary value problem to obtain boundary value problems for the Helmholtz-type equations.
2. Build an effective solver for stationary problems.
3. Reconstruct time-domain solution via numerical inversion of the Laplace transform.

One approach to approximating the inverse Laplace transform was proposed in [13]. If F can be analytically continued to the set $\mathbb{C} \setminus \Sigma_\delta$, where

$$\Sigma_\delta = \{s \in \mathbb{C} : |\arg(-s)| \le \delta, \quad 0 < \delta < \frac{\pi}{2}\}$$

and there exists $M > 0$ such that

$$|F(s)| \le \frac{M}{|s|}, \quad s \in \mathbb{C} \setminus \Sigma_\delta,$$

then to approximate the inverse Laplace transform of function F, a quadrature formula is proposed based on the use of sinc quadrature for integral (5) with a special integration contour (see Figure 1)

$$\gamma(\omega) = \lambda\big(1 - \sin(\alpha + i\omega)\big), \quad \omega \in \mathbb{R}. \tag{6}$$

Here, $\lambda > 0, 0 < \alpha < \frac{\pi}{2} - \delta$ are arbitrary parameters that define the geometry of contour (6).

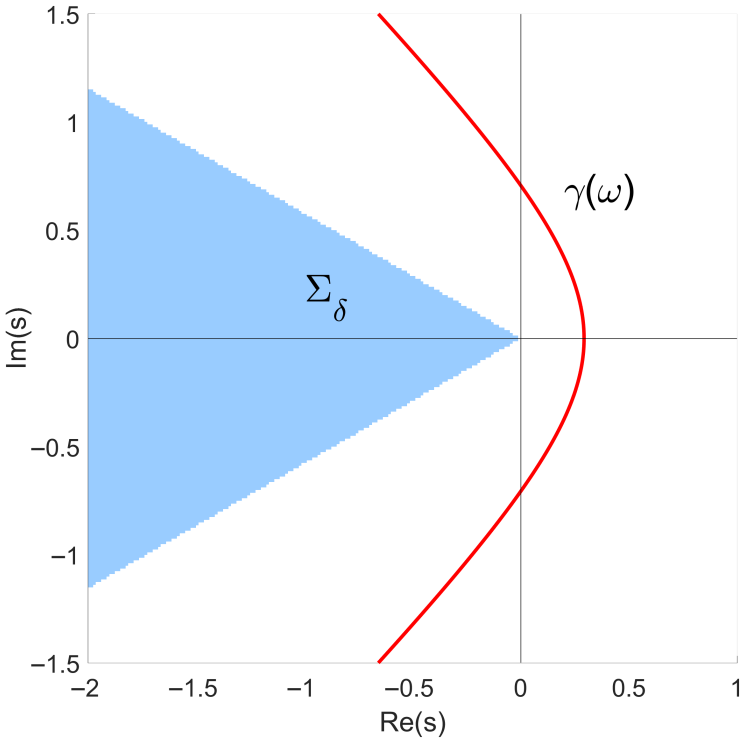

Figure 1. Set Σ_δ and integration contour $\gamma(\omega)$, $\delta = \pi/6$, $\alpha = \pi/4$, $\lambda = 1$.

Using contour (6) to parametrize integral (5), we obtain

$$\mathcal{L}_s^{-1}(F) = f(t) = -\frac{1}{2\pi i}\int_{-\infty}^{\infty} e^{\gamma(\omega)t}F(\gamma(\omega))\gamma'(\omega)d\omega. \tag{7}$$

Let $N_t > 0$, $N_t \in \mathbb{N}$, $h_N = \ln N_t / N_t$, $\omega_j = h_N j$, $j = -N_t, \ldots, N_t$. Integral (7) can be approximated using the following quadrature formula [13]

$$f(t) \approx (T_{N_t}F)(t) = \frac{h_N}{2\pi i}\sum_{j=-N_t}^{N_t} e^{\gamma(\omega_j)t}F(\gamma(\omega_j))\gamma'(\omega_j). \tag{8}$$

Let us denote $s_j = \gamma(\omega_j)$ and $\gamma_j = h_N\gamma'(\omega_j)/2\pi i$; then, we obtain

$$f(t) \approx (T_{N_t}F)(t) = \sum_{j=-N_t}^{N_t} \gamma_j e^{ts_j}F(s_j). \tag{9}$$

Note that when computing $T_{N_t}F$ for different values of t, one can use the same set of values $F(s_j)$. The approximation error of (9) is shown to behave like $\mathcal{O}\left(e^{-cN_t/\ln N_t}\right)$ and is stable to the perturbations of $F(s_j)$. This is especially important when values $F(s_j)$ are computed numerically [13].

Since the solution of the non-stationary problem (1)–(3) u is bounded with respect to the time variable, i.e., its order of growth is equal to 0, the Laplace transform with respect to time can be applied to both parts of Equation (1). Taking into account property $\mathcal{L}_t(f'(t)) = sF(s) - f(0)$ [21] and the zero initial condition, we obtain the following equation for the Laplace image $U_s(x) = \mathcal{L}_t(u(x,t))$

$$\Delta U_s(x) - sU_s(x) = 0, \quad x \in D. \tag{10}$$

On the boundary of the domain, the function U_s satisfies the following condition

$$U_s(x) = G_s(x), \quad x \in \Gamma, \tag{11}$$

where $G_s(x) = \mathcal{L}_t(g(x,t))$. Thus, for U_s we get a boundary value problem (10) and (11) for the Helmholtz equation with a complex wavenumber.

Applying the described approach for the inverse Laplace transform, in order to find an approximate solution of problem (1)–(3), it is necessary to compute

$$U_j(x) = U_{s_j}(x),\ j = -N_t,\ \ldots, N_t,\ x \in D,$$

that is, to solve a set of $2N_t + 1$ problems (10) and (11) for $s = s_j$

$$\Delta U_j(x) - s_j U_j(x) = 0, \quad x \in D, \tag{12}$$

$$U_j(x) = G_j(x), \quad x \in \Gamma. \tag{13}$$

Here, $G_j = G_{s_j}$. It is important to emphasize that problems (12) and (13) are independent of each other, enabling their parallel solution.

In [7,14], it was shown that the image of the solution to the heat problem U_s, as a function of the complex argument s, could be analytically continued to the set $Z = \mathbb{C} \setminus (-\infty, 0]$, and there existed a constant $M > 0$ such that

$$|U_s(\cdot)| \le \frac{M}{|s|}, \quad s \in Z.$$

Thus, in our case, we can apply the approach from [13] and use contour (6) for any $\lambda > 0$ and $0 < \alpha < \frac{\pi}{2}$.

Note that in order to solve problems (12) and (13), it is necessary to have boundary functions G_j, i.e., have the Laplace image G_s of the original boundary condition g. If G_s is not available in a closed form, it can be approximated using various techniques, including using Laguerre polynomials or exponential sums' expansions of the original function [22,23], approximation of the original function by rational functions [24], applying quadrature rules to the Laplace transform integral [25] and others. The approximation of G_s is beyond the scope of the current article, and we use examples of g with a known Laplace transform for the numerical experiments.

Recalling problems (12) and (13) are 3D stationary boundary value problems, it is easy to see that solving them numerically may pose a significant computational effort. The main motivation for this article was to suggest certain ideas for decreasing the amount of computational work, as described further.

2.1. Reducing the Number of Stationary Problems

It is easy to notice that $\omega_{-j} = -\omega_j, j = 1, \ldots, N_t$.

Then,

$$s_{-j} = \gamma(\omega_j) = \lambda\big(1 - \sin(\alpha + i\omega_j)\big) =$$

$$= \lambda\big(1 - \sin(\alpha - i\omega_{N_t - j})\big) = \overline{\lambda\big(1 - \sin(\alpha + i\omega_{N_t - j})\big)} = \overline{s_j}, \quad j = 1, \ldots, N_t, \tag{14}$$

where $\overline{z}$ denotes the complex conjugate of z. We use the fact that $\overline{\sin(z)} = \sin(\overline{z})$ for any complex z [26].

Thus, quadrature nodes (14) are pairwise conjugate, except for node s_0. This allows us to reduce the solution of the set of $2N_t + 1$ stationary problems to $N_t + 1$ problems.
We show that

$$U_{-j}(x) = \overline{U_j(x)}, \quad j = 1, \ldots, N_t.$$

Theorem 1. *Assume $D \subset \mathbb{R}^3$ is a simply connected region with a smooth boundary Γ from C^2, $G \in C(\Gamma)$ and complex-valued parameter $s \in \mathbb{C} \setminus (-\infty, 0]$. Let $U \in C^2(D) \cap C(\overline{D})$ be a solution of the problem*

(a) $\Delta U(x) - sU(x) = 0, \quad x \in D,$
(b) $U(x) = G(x), \quad x \in \Gamma.$

Then, $\overline{U} \in C^2(D) \cap C(\overline{D})$ *is a solution of the problem*

(c) $\Delta\overline{U(x)} - \bar{s}\,\overline{U(x)} = 0, \quad x \in D,$
(d) $\overline{U(x)} = \overline{G(x)}, \quad x \in \Gamma.$

Proof. Statement (d) follows directly from (b). Let us show that (c) follows from (a). We denote

$$s = a + ib, \quad U(x) = V(x) + iW(x), \ x \in D,$$
$$\bar{s} = a - ib, \quad \overline{U(x)} = V(x) - iW(x), \ x \in D.$$

Then, (a) can be written as

$$\Delta V + i\Delta W = aV - bW + i(bV + aW)$$

Thus,

$$\Delta V = aV - bW, \ \Delta W = bV + aW.$$

Then,

$$\Delta\overline{U} = \Delta V - i\Delta W =$$
$$= aV - bW - ibV - iaW =$$
$$= (a - ib)V - i(a - ib)W =$$
$$= (a - ib)(V - iW) = \bar{s}\,\overline{U},$$

which proves statement (c). □

Corollary 1. *Solutions of problems* (12) *and* (13) *with indices* $-j$ *and* j *are complex conjugates*

$$U_{-j}(x) = \overline{U_j(x)}, \quad j = 1, \ldots, N_t, \ x \in D.$$

Proof. Using the well-known fact that $F(\bar{s}) = \overline{F(s)}$ (for real valued $f(t)$ [26]), it is easy to see that the boundary conditions of the problems with indices $-j$ and j are complex conjugates. Since $s_{-j} = \overline{s_j}$, it follows from Theorem 1 that the solutions of problems (12) and (13) with indices $-j$ and j are also complex conjugates. □

Thus, it is sufficient to solve the stationary problems for indices $j = 0, \ldots, N_t$, and the solutions for indices $j = -N_t, \ldots, -1$ can be obtained automatically from the Corollary 1.

2.2. Integration Contour Parameters Optimization

As mentioned earlier, integration contour (6) depends on parameters $\lambda > 0$ and $0 < \alpha < \frac{\pi}{2}$. Figures 2 and 3 show the influence of parameters α and λ on the shape of the contour and placement of the nodes for $N_t = 4$.

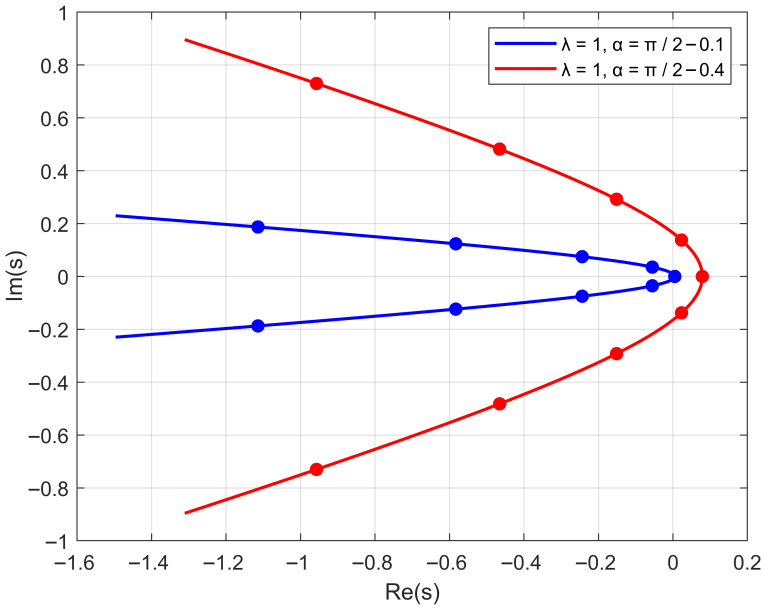

Figure 2. Influence of α on the integration contour: when α gets closer to $\pi/2$, the contour branches get closer to the real axis.

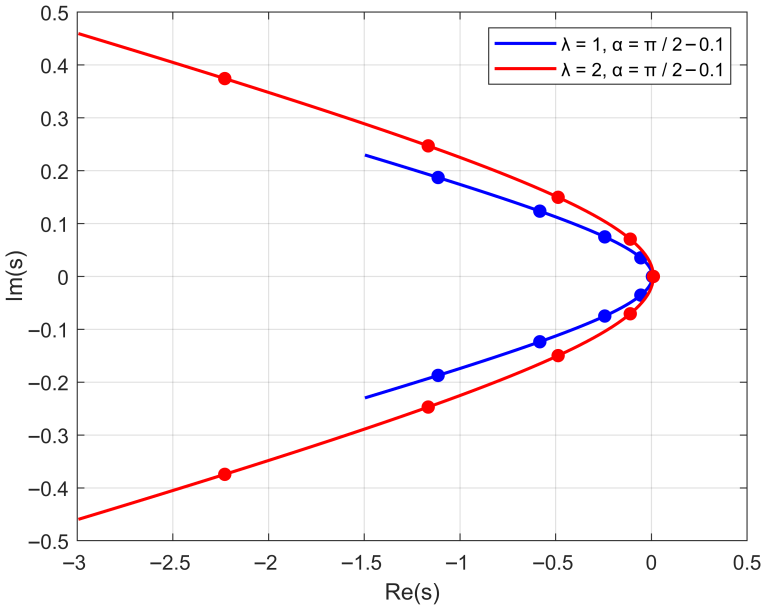

Figure 3. Influence of λ on the integration contour: when λ is larger, the contour is "scaled out", and nodes are spread further along the branches.

Since the approximate solution of the 3D stationary problems requires a large number of computations, it makes sense to select parameters α and λ in such a way as to reduce the expected error.

To find parameters α and λ for which the error is minimized, we define search intervals for the optimal values of α and λ and construct a uniform grid of test values for them:

$$\alpha \in [\alpha_0, \alpha_1] \subset (0; \pi/2), \quad \lambda \in [\lambda_0, \lambda_1] \subset (0; \infty),$$

$$\alpha_\nu = \alpha_0 + \nu h_\alpha, \quad \nu = 0, \ldots, N_\alpha, N_\alpha \in \mathbb{N}, \quad h_\alpha = (\alpha_1 - \alpha_0)/N_\alpha, \tag{15}$$

$$\lambda_\mu = \lambda_0 + \mu h_\lambda, \quad \mu = 0, \ldots, N_\lambda, N_\lambda \in \mathbb{N}, \quad h_\lambda = (\lambda_1 - \lambda_0)/N_\lambda. \tag{16}$$

We fix certain values of t and N_t and select a Laplace transform pair of test functions u^T and U_s^T. It is natural to select u^T to be similar to the behavior of the boundary condition g. Then, for each pair of values $(\alpha_\nu, \lambda_\mu)$, we compute the absolute or relative errors E_{abs} and E_{rel} of the numerical Laplace transform inversion (9) for U_s^T and find the values $(\alpha_{\min}, \lambda_{\min})$ for which

$$E_{abs,min} = min\{E_{abs} \mid (\alpha_{\nu,\lambda_\mu}), \nu = 0, \ldots, N_\alpha, \mu = 0, \ldots, N_\lambda\}, \tag{17}$$

$$E_{rel,min} = min\{E_{rel} \mid (\alpha_{\nu,\lambda_\mu}), \nu = 0, \ldots, N_\alpha, \mu = 0, \ldots, N_\lambda\}. \tag{18}$$

The obtained contour parameters $(\alpha_{\min}, \lambda_{\min})$ are then used to define quadrature nodes s_j and solve $N_t + 1$ stationary problems. We do not provide an explicit recipe to define $[\alpha_0, \alpha_1]$ and $[\lambda_0, \lambda_1]$. For $[\alpha_0, \alpha_1]$ it seems natural to define α_0 close to 0 and α_1 close to $\pi/2$ and thus "scan" most of the $(0; \pi/2)$ interval. For $[\lambda_0, \lambda_1]$, it seems natural to define λ_0 close to 0, and it is empirically observed that increasing λ_1 prevents us from finding different λ_{min}'s after certain values of λ_1. This is intuitively supported by understanding that for large values of λ, nodes s_j quickly start to extend far into the left half-plane and their contribution in sum (9) becomes negligible.

3. Solver for Stationary Boundary Value Problems

In this section, we consider the numerical solution of the stationary problems (12)–(13). We apply the BIE method with later application of the Nyström method based on the quadrature rules for surface integrals proposed by Wienert [20].
For brevity, we rewrite problems (12) and (13) as

$$\Delta U_s(x) - sU_s(x) = 0, \quad x \in D,\ s \in \{s_j,\ j = 0, \ldots, N_t\}, \tag{19}$$

$$U_s(x) = G_s(x), \quad x \in \Gamma. \tag{20}$$

The fundamental solution of Equation (19) has the following form [27]

$$\Phi_s(x, y) = \frac{1}{4\pi} \frac{e^{-\sqrt{s}|x-y|}}{|x-y|}, \quad x, y \in \mathbb{R}^3,\ x \neq y,\ Re(\sqrt{s}) > 0. \tag{21}$$

Since $s \notin (-\infty, 0]$, it is known that under suitable assumptions on the boundary Γ and for sufficiently smooth boundary data G_s, the solution of the Dirichlet problem exists and is unique; see [27] and references therein. The solution of (19) can be written in the form of a double-layer potential

$$U_s(x) = \int_\Gamma \varphi(y)\Phi_{\nu,s}(x, y)ds(y), \quad x \in \Gamma, \tag{22}$$

where $\Phi_{\nu,s}(x, y) = \frac{\partial \Phi_s(x,y)}{\partial \nu(y)}$, $\varphi \in C(\Gamma)$ is the potential density, and ν is the unit outward normal vector to Γ.

Potential (22) is a solution of problems (12) and (13) if the density φ is a solution of the Fredholm integral equation of the second kind

$$-\frac{1}{2}\varphi(x) + \int_\Gamma \varphi(y)\Phi_{\nu,s}(x, y)ds(y) = G_s(x), \quad x \in \Gamma. \tag{23}$$

For any $G_s \in C(\Gamma)$, Equation (23) has a unique solution φ in $C(\Gamma)$ [27].

Since $\Gamma = \{x = q(\hat{x}), \hat{x} \in \mathbb{S}^2)\}$, we can obtain the parametrized integral equation on $\mathbb{S}^2$

$$-\frac{1}{2}\psi(\hat{x}) + \int_{\mathbb{S}^2} \psi(\hat{y})\, K(\hat{x},\hat{y})\, ds(\hat{y}) = \hat{G}_s(\hat{x}), \quad \hat{x} \in \mathbb{S}^2, \tag{24}$$

where we denoted $\psi(\hat{x}) = \varphi(q(\hat{x}))$, $\hat{G}_s(\hat{x}) = G_s(q(\hat{x}))$, $\hat{x} \in \mathbb{S}^2$ and

$$K(\hat{x},\hat{y}) = \Phi_{\nu,s}(q(\hat{x}), q(\hat{y}))J(\hat{y}), \quad \hat{x},\hat{y} \in \mathbb{S}^2,\ \hat{x} \neq \hat{y}.$$

Function K is a weakly singular integral kernel that can be rewritten in the form

$$K(\hat{x},\hat{y}) = \frac{M(\hat{x},\hat{y})}{|\hat{x}-\hat{y}|}, \quad \hat{x},\hat{y} \in \mathbb{S}^2,\ \hat{x} \neq \hat{y},$$

where

$$M(\hat{x},\hat{y}) = \frac{e^{-\sqrt{s}|q(\hat{x})-q(\hat{y})|}}{4\pi} \frac{(q(\hat{x})-q(\hat{y}),\, \nu(q(\hat{y})))}{|q(\hat{x})-q(\hat{y})|^2} \frac{|\hat{x}-\hat{y}|J(\hat{y})}{|q(\hat{x})-q(\hat{y})|} \left(\sqrt{s}|q(\hat{x})-q(\hat{y})|+1\right).$$

Note that due to the analyticity of q, the well-posedness of (23) also applies to (24). In order to discretize (24), we consider the quadrature rules proposed by Wienert [20]. For a given space discretization parameter $N \in \mathbb{N}$, the following values are defined

$$\hat{p}_{\beta,\mu} = p(\vartheta_\beta, \varphi_\mu), \vartheta_\beta = \arccos \xi_\beta,\ \varphi_\mu = \frac{\pi}{N}\mu, \tag{25}$$

$$w_\beta^{(1)} = \frac{2\pi}{N(1-\xi_\beta^2)\left(P_N'(\xi_\beta)\right)^2}, \quad \beta = 1,\ldots,N,\ \mu = 0,\ldots,2N-1.$$

where $\xi_1 < \cdots < \xi_N$ are the zeros of the Legendre polynomials P_N [28].

For a given function $f \in C(\mathbb{S}^2 \setminus \{(0,0,\pm 1)\})$, approximation $A_N f$ is defined as

$$(A_N f)(\hat{x}) = \sum_{\beta=1}^{N} \sum_{\mu=0}^{2N-1} w_\beta^{(1)} f(\hat{p}_{\beta,\mu})\, a_{\beta,\mu}(\hat{x}), \tag{26}$$

where $a_{\beta,\mu}(\hat{x}) = \sum_{n=0}^{N-1} \frac{2n+1}{4\pi} P_n(\hat{x}\cdot\hat{p}_{\beta,\mu})$, and by $\hat{x}\cdot\hat{p}_{\beta,\mu}$ we denote a scalar product of two vectors. Note that the poles are excluded from the continuity requirements, since values of the parametrized functions $f \circ p$ at the poles may depend on the direction of approach (i.e., specific value of φ) and may be not continuous at the poles.
For non-singular integrands, the following quadrature rule is suggested

$$\int_{\mathbb{S}^2} f(\hat{y})\, ds(\hat{y}) \approx \int_{\mathbb{S}^2} (A_N f)(\hat{y})\, ds(\hat{y}) = \sum_{\beta=1}^{N} \sum_{\mu=0}^{2N-1} w_\beta^{(1)} f(\hat{p}_{\beta,\mu}). \tag{27}$$

For weakly singular integrands, the following quadrature rule can be used

$$\int_{\mathbb{S}^2} \frac{f(\hat{y})}{|\hat{n}_p-\hat{y}|}\, ds(\hat{y}) \approx \int_{\mathbb{S}^2} \frac{(A_N f)(\hat{y})}{|\hat{n}_p-\hat{y}|}\, ds(\hat{y}) = \sum_{\beta=1}^{N} \sum_{\mu=0}^{2N-1} w_\beta^{(2)} f(\hat{p}_{\beta,\mu}), \tag{28}$$

where $w_\beta^{(2)} = w_\beta^{(1)} \sum_{n=0}^{N-1} P_n(\xi_\beta)$ and $\hat{n}_p = (0,0,1)$.

Both quadratures are obtained by approximating the regular part of the integrand via approximation A_N and then using exact integration. According to results in [20], these quadrature rules have super-algebraic or even exponential convergence order, depending on the smoothness of f.

By simple substitution, the quadrature rule (28) can be extended to a more general case

$$\int_{\mathbb{S}^2} \frac{f(\hat{y})}{|\hat{x}-\hat{y}|}\, ds(\hat{y}) = \int_{\mathbb{S}^2} \frac{f(T_{\hat{x}}^{-1}\hat{y})}{|\hat{n}_p-\hat{y}|}\, ds(\hat{y}) \approx \sum_{\beta=1}^{N}\sum_{\mu=0}^{2N-1} w_\beta^{(2)} f(T_{\hat{x}}^{-1}\hat{p}_{\beta,\mu}),\ \hat{x}\in\mathbb{S}^2, \tag{29}$$

where $T_{\hat{x}}$ is usually a rotation, such that $T_{\hat{x}}\hat{x} = \hat{n}_p$, see [20].

Applying (29) to the integral in (24), for $\tilde{\psi} \approx \psi$, we get an approximation equation

$$-\frac{1}{2}\tilde{\psi}(\hat{x}) + \sum_{\beta=1}^{N}\sum_{\mu=0}^{2N-1} w_\beta^{(2)} \tilde{\psi}(T_{\hat{x}}^{-1}\hat{p}_{\beta,\mu})\, M(\hat{x}, T_{\hat{x}}^{-1}\hat{p}_{\beta,\mu}) = \hat{G}_s(\hat{x}), \quad \hat{x}\in\mathbb{S}^2. \tag{30}$$

We observe that (30) contains values of the density $\tilde{\psi}$ in the rotated nodes $T_{\hat{x}}^{-1}\hat{p}_{\beta,\mu}$. In order to be able to construct a system of linear equations, we replace $\tilde{\psi}(T_{\hat{x}}^{-1}\hat{p}_{\beta,\mu})$ with its approximation by A_N (26)

$$\tilde{\psi}(T_{\hat{x}}^{-1}\hat{p}_{\beta,\mu}) \approx (A_N\tilde{\psi})(T_{\hat{x}}^{-1}\hat{p}_{\beta,\mu}) = \sum_{\beta'=1}^{N}\sum_{\mu'=0}^{2N-1} w_{\beta'}^{(1)} \tilde{\psi}(\hat{p}_{\beta',\mu'}) a_{\beta',\mu'}(T_{\hat{x}}^{-1}\hat{p}_{\beta,\mu}). \tag{31}$$

Substituting (31) back into (30), we get

$$-\frac{1}{2}\tilde{\psi}(\hat{x}) + \sum_{\beta'=1}^{N}\sum_{\mu'=0}^{2N-1} \tilde{\psi}(\hat{p}_{\beta',\mu'}) w_{\beta',\mu'}^{(3)}(\hat{x}) = \hat{G}_s(\hat{x}), \quad \hat{x}\in\mathbb{S}^2, \tag{32}$$

where $w_{\beta',\mu'}^{(3)}(\hat{x}) = w_{\beta'}^{(1)} \sum_{\beta=1}^{N}\sum_{\mu=0}^{2N-1} w_\beta^{(2)}\, M(\hat{x}, T_{\hat{x}}^{-1}\hat{p}_{\beta,\mu}) a_{\beta',\mu'}(T_{\hat{x}}^{-1}\hat{p}_{\beta,\mu})$.

Collocating the Equation (32) in the nodes $\hat{p}_{\beta_2,\mu_2},\ \beta_2 = 1,\dots,N,\ \mu_2 = 0,\dots,2N-1$, we get a $2N^2 \times 2N^2$ system of linear equations for the unknown values $\tilde{\psi}(\hat{p}_{\beta_2,\mu_2})$

$$-\frac{1}{2}\tilde{\psi}(\hat{p}_{\beta_2,\mu_2}) + \sum_{\beta'=1}^{N}\sum_{\mu'=0}^{2N-1} \tilde{\psi}(\hat{p}_{\beta',\mu'}) w_{\beta',\mu'}^{(3)}(\hat{p}_{\beta_2,\mu_2}) = \hat{G}_s(\hat{p}_{\beta_2,\mu_2}). \tag{33}$$

After solving (33), the approximate solutions of problems (19) and (20) for parameter $s = \{s_j, j = 0,\dots,N_t\}$ can be found by applying the quadrature rule (27) to (22)

$$U_{j,N}(x) = \sum_{\beta_2=1}^{N}\sum_{\mu_2=0}^{2N-1} w_{\beta_2}^{(1)} \tilde{\psi}_j(\hat{p}_{\beta_2,\mu_2}) \Phi_{\nu,s_j}(x, q(\hat{p}_{\beta_2,\mu_2})) J(\hat{p}_{\beta_2,\mu_2}), \quad x\in D,\ j = 0,\dots,N_t, \tag{34}$$

where $\tilde{\psi}_j(\hat{p}_{\beta_2,\mu_2}) = \tilde{\psi}(\hat{p}_{\beta_2,\mu_2})$ for the parameter value $s = s_j$.

Having solved a set of problems (19) and (20), we can construct the approximate solution of the original non-stationary problems (1)–(3)

$$u(x,t) \approx u_{N_t,N}(x,t) = \sum_{j=0}^{N_t} \gamma_j e^{ts_j} U_{j,N}(x) + \sum_{j=-N_t}^{-1} \gamma_j e^{ts_j} \overline{U_{-j,N}(x)},\ (x,t)\in D\times(0,\infty). \tag{35}$$

As previously mentioned, the error rate of the numerical inversion of the Laplace transform behaves like $\mathcal{O}\left(e^{-cN_t/\ln N_t}\right)$ and is stable to perturbations of U_j values. In our case, these perturbations are created by the fact that U_j are approximated by $U_{j,N}$, which in practice

exhibits a super-algebraic convergence rate for sufficiently smooth surfaces and boundary conditions. As result, when N_t and N are selected in a balanced way, the overall error rate of the original non-stationary problem is super-algebraic, which is shown in the following numerical experiments.

4. Numerical Experiments

We consider the following examples of regions $D_k,\ k = 1,2$ and their boundaries Γ_k to perform numerical experiments (see Figure 4)

$$\Gamma_1 = \{r_1(\theta,\varphi)(\sin\theta\cos\phi,\ \sin\theta\sin\phi,\ \cos\theta),\ (\theta,\phi) \in [0,\pi]\times[0,2\pi)\},$$

$$r_1(\theta,\varphi) = A_1\left(0.6 + \sqrt{4.25 + 2\cos 3\theta}\right),\ A_1 \in \mathbb{R} > 0,$$

$$\Gamma_2 = \{r_2(\theta,\varphi)(\sin\theta\cos\phi,\ \sin\theta\sin\phi,\ \cos\theta),\ (\theta,\phi) \in [0,\pi]\times[0,2\pi)\},$$

$$r_2(\theta,\varphi) = A_2\sqrt{0.8 + 0.2(\cos(2\varphi)-1)(\cos(4\theta)-1)},\ A_2 \in \mathbb{R} > 0.$$

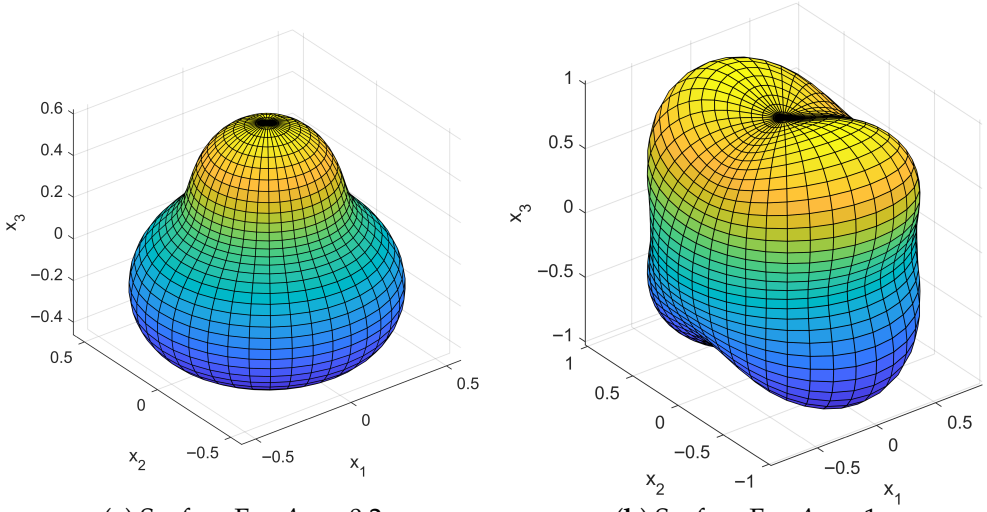

(**a**) Surface $\Gamma_1,\ A_1 = 0.2$ (**b**) Surface $\Gamma_2,\ A_2 = 1$

Figure 4. Boundary surfaces.

Note that when defining specific surfaces Γ using mapping $q : \mathbb{S}^2 \to \Gamma$, it is possible to use spherical or Cartesian coordinates to describe points on the unit sphere. For the mentioned surfaces Γ_1 and Γ_2, we used spherical coordinates.

4.1. Inverse Laplace Transform

Here, we test the numerical inversion of the Laplace transform and suggested optimizations. Let us consider the fundamental solution of the heat Equation (1)

$$\tilde{G}(x,y,t) = \frac{1}{\sqrt{4\pi t^3}} e^{\frac{|x-y|^2}{4t}},\quad x,y \in R^3,\ x \neq y,\ t > 0. \tag{36}$$

The Laplace image of $\tilde{G}$ is a fundamental solution of the Helmholtz Equation (10)

$$\mathcal{L}_t(\tilde{G}(x,y,t)) = \int_0^\infty e^{-st}\tilde{G}(x,y,t)dt = \Phi_s(x,y).$$

For a given source point $y^* \notin D_1$, function

$$w(x,t) = \tilde{G}(x,y^*,t),\ x \in D_1,\ y^* \notin D_1,\ t > 0,$$

is an exact solution of Equation (1), and its Laplace transform $W_s(x) = \Phi_s(x, y^*)$ is an exact solution of Equation (10). Clearly, Theorem 1 holds true in this case, so the values of W_s can be computed only at nodes $s_j,\ j = 0, \ldots, N_t$.

To test the effect of the α, λ selection, we chose some random values of $\tilde{\alpha}, \tilde{\lambda}$ and calculated the absolute error $E_{abs} = |T_{N_t} W_s - w|$ for the approximate computation of the inverse Laplace transform. Then, we used the optimization process (17) to find the optimal parameters α_{min} and λ_{min} and calculated the absolute error $E_{abs,min}$. For the search intervals' bounds, the following values were used: $\alpha_0 = 0.01$, $\alpha_1 = \pi/2 - 0.01$, $\lambda_0 = 0.1$ and $\lambda_1 = 20$. The rationale for the $[\alpha_0, \alpha_1]$ selection was to cover most of the $(0, \pi/2)$ interval. The rationale for the $[\lambda_0, \lambda_1]$ selection was based on numerical experiments, where the optimal λ_{min} value was usually found within the $[1, 10]$ range. Tables 1 and 2 show the comparison of $E_{abs,min}$ and E_{abs} for the different values of x, y^* and t.

Table 1. Errors $E_{abs,min}$ and E_{abs} for $x = (0.1, 0.1, 0.2),\ y^* = (0, 0, 5),\ t = 2,\ N_\alpha = 20,\ N_\lambda = 40$.

N_t	$E_{abs,min}$	α_{min}	λ_{min}	E_{abs}	$\tilde{\alpha}$	$\tilde{\lambda}$
2	1.27×10^{-8}	0.989450	9.794872	2.88×10^{-4}	$\pi/2 - 0.2$	1
4	2.71×10^{-11}	0.826209	5.712821	2.00×10^{-5}	$\pi/2 - 0.2$	1
8	1.01×10^{-15}	1.071071	3.671795	5.56×10^{-7}	$\pi/2 - 0.2$	1
16	5.45×10^{-20}	1.071071	5.712821	8.75×10^{-11}	$\pi/2 - 0.2$	1

Table 2. Errors $E_{abs,min}$ and E_{abs} for $x = (0.1, 0.05, 0.05),\ y^* = (0, 0, 4),\ t = 1.5,\ N_\alpha = 30,\ N_\lambda = 60$.

N_t	$E_{abs,min}$	α_{min}	λ_{min}	E_{abs}	$\tilde{\alpha}$	$\tilde{\lambda}$
2	6.44×10^{-8}	1.212716	8.869492	2.98×10^{-4}	$\pi/2 - 0.2$	1
4	1.16×10^{-8}	1.096689	4.822034	1.82×10^{-4}	$\pi/2 - 0.2$	1
8	3.11×10^{-15}	1.058013	6.171186	3.83×10^{-6}	$\pi/2 - 0.2$	1
16	1.04×10^{-19}	1.077351	9.206780	5.59×10^{-9}	$\pi/2 - 0.2$	1

The obtained results support the expected error rates. Note that the tested $(\alpha_{min}, \lambda_{min})$ search routine is computationally fast (it involves $N_\alpha \times N_\lambda$ Laplace inversions), and its cost is negligible compared to the computational effort of solving the stationary 3D problem. Comparing specific values in Tables 1 and 2, one could expect a significant reduction in necessary N_t, i.e., the number of stationary problems to solve.

4.2. Stationary Problem

In this section, we test the numerical solution of the stationary problems (10) and (11) using the BIE method described in Section 3. As a sample boundary condition, we chose G_s as the narrowing of the fundamental solution $\Phi_s(\cdot, y^*)$ onto Γ with a source point y^* outside the region D_k. In this case, the exact solution of problems (10) and (11) is

$$U_s(x) = \Phi_s(x, y^*), \quad x \in D_k,\ y^* \notin D_k,\ k = 1, 2.$$

Let $y^* = (0, 0, 5) \notin D_k,\ k = 1, 2$. To measure the accuracy of the numerical approximation, we used the following discrete L_2 error

$$E_{L_2} = \frac{1}{\tilde{N}} \left(\sum_{m=1}^{\tilde{N}} \sum_{j=1}^{\tilde{N}} \left| U_s(x_{m,j}) - U_{s,N}(x_{m,j}) \right|^2 \right)^{1/2},$$

where $U_{s,N}$ is the approximate solution obtained by (34) and $\tilde{N} = 10$. The test points $x_{m,j}$ were uniformly distributed on a diminished artificial surface located within the solution domain, according to the following rule

$$x_{m,j} = 0.5 r_k(\theta_m, \phi_j) p(\theta_m, \phi_j),\ \theta_m = \frac{\pi}{\tilde{N}+1} m,\ \phi_j = \frac{2\pi}{\tilde{N}} j,\ \ m, j = 1, \ldots, \tilde{N},\ k = 1, 2.$$

Tables 3 and 4 and show the error E_{L_2} for the two test surfaces, different equation parameter values s and space discretization parameter N.

Table 3. Discrete E_{L_2} error for the case $D = D_1$.

N	Nodes	$s_1 = 1$	$s_2 = 0.5 - 3i$	$s_3 = 2 + 5i$
4	32	4.35×10^{-6}	2.41×10^{-6}	5.43×10^{-8}
8	128	6.12×10^{-7}	3.51×10^{-7}	3.26×10^{-9}
16	512	2.56×10^{-9}	6.80×10^{-10}	2.27×10^{-11}
32	2048	7.32×10^{-12}	3.66×10^{-12}	4.24×10^{-12}

Table 4. Discrete E_{L_2} error for the case $D = D_2$.

N	Nodes	$s_1 = 1$	$s_2 = 0.5 - 3i$	$s_3 = 2 + 5i$
4	32	3.75×10^{-6}	8.92×10^{-8}	1.37×10^{-8}
8	128	4.74×10^{-7}	1.27×10^{-8}	2.43×10^{-9}
16	512	6.31×10^{-9}	5.83×10^{-9}	1.29×10^{-10}
32	2048	7.14×10^{-11}	4.29×10^{-11}	3.92×10^{-11}

The obtained results support the error rates provided by Wienert [20].

4.3. Non-Stationary Problem

In this subsection, we test the numerical solution of non-stationary problem (1)–(3). The first example shows a case with an exactly known solution. The second example shows a case where the exact solution is not known, but the boundary condition (3) has a Laplace transform available in closed form. If the boundary condition does not possess a Laplace transform in the closed form, it is suggested to apply some of the Laplace transform approximation methods briefly mentioned in Section 2. For all examples, as suggested in Section 2, we solved only $N_t + 1$ stationary problems to provide approximate values $U_{j,N}$ for the numerical inversion of the Laplace transform. We also applied the selection technique for parameters (α, λ) described in Section 2 and tested in Section 4.1.

4.3.1. Example with an Exactly Known Solution

As a sample boundary condition (3), we chose a narrowing of the fundamental solution (36) onto Γ_1

$$g(x,t) = \tilde{G}(x, y^*, t),\ (x,t) \in \Gamma_1 \times (0, \infty),\ y^* \notin D_1.$$

In this case, the exact solution of problem (1)–(3) is

$$u(x,t) = \tilde{G}(x, y^*, t), \quad (x,t) \in D_1 \times (0, \infty),\ y^* \notin D_1.$$

Let $y^* = (0, 0, 5),\ x_0 = (0.1, 0.1, 0.2)$. Table 5 shows the absolute error $\widetilde{E}_{abs}(t) = |u(x_0, t) - u_{N_t,N}(x_0, t)|$ for the different values of t and discretization parameters N_t, N. Note that for each test point t, contour parameters α and λ were selected using optimization process (17)
.

Table 5. Absolute error $\widetilde{E}_{abs}$, $D = D_1$.

N_t	N	$t = 2$	$t = 2.2$	$t = 2.5$
2	4	2.136812×10^{-5}	2.462481×10^{-5}	2.837609×10^{-5}
	8	1.946759×10^{-6}	2.188658×10^{-6}	2.331827×10^{-6}
	16	2.325619×10^{-8}	2.773015×10^{-10}	9.600292×10^{-8}
	32	1.540043×10^{-8}	8.910118×10^{-9}	8.651947×10^{-8}
4	4	2.137816×10^{-5}	2.461644×10^{-5}	2.844138×10^{-5}
	8	1.962045×10^{-6}	2.179749×10^{-6}	2.418113×10^{-6}
	16	7.838391×10^{-9}	8.531891×10^{-9}	9.433593×10^{-9}
	32	1.884036×10^{-11}	5.333509×10^{-11}	1.013018×10^{-10}
8	4	2.137815×10^{-5}	2.461638×10^{-5}	2.844134×10^{-5}
	8	1.962032×10^{-6}	2.179657×10^{-6}	2.418072×10^{-6}
	16	7.851940×10^{-9}	8.624379×10^{-9}	9.475018×10^{-9}
	32	5.286807×10^{-12}	8.816986×10^{-12}	1.190821×10^{-11}

To verify that the obtained error rates agree with error rates of the numerical Laplace inversion and stationary problems solution, Table 6 highlights decimal exponents of the absolute errors for the same point $x_0 = (0.1, 0.1, 0.2)$ and $t = 2$.

Table 6. Error rate comparison.

Laplace Inversion		**Stationary**		**Non-Stationary**	
N_t	$log_{10}(E_{abs})$	N	$log_{10}(E_{L_2})$	N_t, N	$log_{10}(\widetilde{E}_{abs})$
2	-8	16	-10	2, 16	-8
4	-11	32	-12	4, 32	-11
8	-15	32	-12	8, 32	-12

It is easy to see that the full discretization of the non-stationary problem results in an error rate defined by the worst error of the Laplace inversion and stationary problem solution, which is expected. It also indicates a balanced selection of N_t and N may provide the best overall result.

4.3.2. Example Without Exactly Known Solution

Let us consider the numerical solution of non-stationary problem (1)–(3) with the following boundary condition

$$g(x,t) = t^2 e^{-t}, \quad (x,t) \in \Gamma_1 \times (0,\infty). \tag{37}$$

For the stationary problems' boundary condition, we used the closed form of the Laplace transform of g

$$G_s(x) = \mathcal{L}_t(g) = \frac{2}{(s+1)^3}, \; x \in \Gamma_1, \; s \in \mathbb{C}, s \neq -1.$$

Table 7 shows the values of the approximate solution of (1)–(3) for different combinations of N_t and N, different points $x \in D_1$ and time points t.

For each combination of x and t, we observe an increasing number of the same decimal digits as N_t and N grow.

Let us consider region D_1 with the scaling parameter of boundary Γ_1 set to $A_1 = 6$. We calculated and plotted the numerical solution of non-stationary problem (1)–(3) with boundary condition (37) over time interval $t \in (0; 10]$ at two points $x_1 = (0, 0, 0)$ and $x_2 = (2.5, 0, 0)$. Note that the two test points were intentionally selected so x_1 was placed "deeper" within the region and point x_2 was closer to the boundary. Parameter A_1 was

intentionally selected to significantly scale up the region in order to observe a time delay in the propagation of the boundary condition behavior inside the region. To produce the plots, we chose a time step $\Delta t = 0.2$ and numerically solved problem (1)–(3) 50 times for each test point using discretization parameters $N_t = 4, N = 8$. The entire computation process took 2–3 min using an average-level PC. This and previous numerical examples were implemented using MATLAB R2024b.

Table 7. Approximate solution for different N_t, N, x and t.

t	N_t	N	$x = (0.1, 0.05, 0.05)$	$x = (0, 0, 0.4)$
1	2	4	0.35246148	0.35659063
	4	8	0.35245882	0.35987086
	4	16	0.35246211	0.35987241
	4	32	0.35246211	0.35987241
3	2	4	0.45384016	0.44480551
	4	8	0.45327121	0.45057778
	4	16	0.45327211	0.45057821
	4	32	0.45327211	0.45057821
5	2	4	0.17317714	0.16828926
	4	8	0.17226425	0.17033565
	4	16	0.17225089	0.17032869
	4	32	0.17225089	0.17032869

As can be seen from Figure 5, boundary condition propagation time delays and peak values at x_1 and x_2 show the expected behavior.

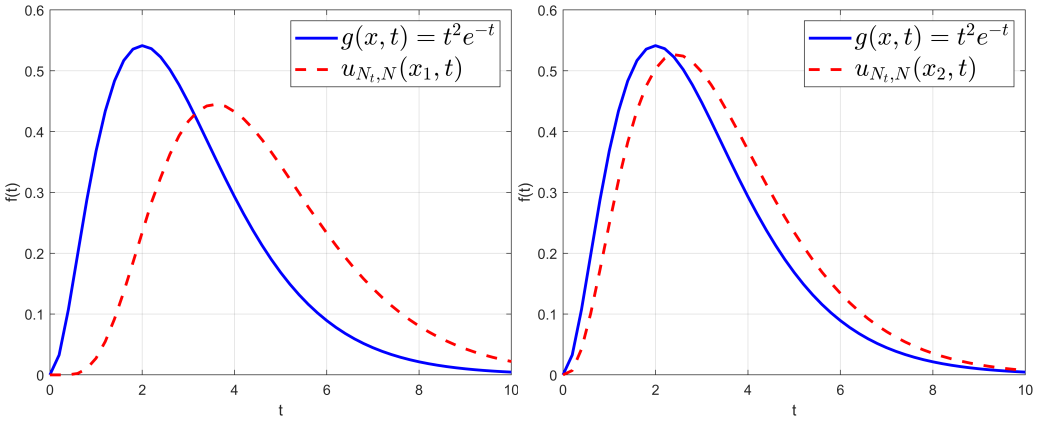

Figure 5. Numerical solution and boundary condition. (**a**) "Deeper" placement of $x_1 = (0, 0, 0)$ showing a bigger time delay in "peak" propagation and bigger difference in peak height. (**b**) Placement of $x_2 = (2.5, 0, 0)$ closer to the boundary showing a smaller time delay in "peak" propagation and difference in peak height.

Finally, we would like to provide a brief comparison of the results of this paper to those of previous studies, namely, to the Chapko & Johansson [6], where an exterior 3D initial BVP was considered, and the authors applied the Laguerre transform for the time discretization. As a result, stationary BVPs for a recurrent sequence of elliptic equations were obtained, and to apply the BIE method, one needs to find the fundamental sequence. The inverse Laguerre transform has the form of the Fourier–Laguerre series, and its summation is a complicated ill-posed problem, especially for long time periods. Comparing the numerical results in both papers, we noticed better levels of the errors were obtained for the reasonably smaller time discretization parameter in case of the Laplace transform.

5. Conclusions

In this article, an effective combination of the Laplace transform and boundary integral equation method for the numerical solution of the 3D initial boundary value problem for the heat equation was proposed and tested.

The optimization of the inverse Laplace transform integration contour parameters was shown to substantially decrease the approximation error, allowing for the reduction in the number of stationary BVPs to achieve a certain level of precision. Moreover, using observed and proven symmetry in the set of boundary value problems, computational work was further reduced by a factor of almost two. As mentioned in the article, due to the independence of the boundary value problems, the proposed approach is also suitable for parallel computing.

The stationary BVPs were solved using the indirect BIE method with application of the Nyström method based on the Wienert quadrature rules for the surface integrals.

The efficiency and feasibility of the suggested two-step approach were confirmed by a set of numerical experiments, testing time and space discretization methods separately and combined.

In future work, the presented approach will be tested with other methods for solving boundary value problems, as well as different equations or types of boundary conditions. Further research of the optimization techniques for the numerical Laplace transform inversion is planned. Another direction of research is to expand the domain types, consider doubly connected regions, etc. Additionally, the described approach will be used for the numerical solution of inverse problems, for example, the lateral Cauchy problem to reconstruct boundary data on part of the domain boundary.

Author Contributions: Both authors contributed equally to the research and preparation of this article. All authors have read and agreed to the published version of the manuscript.

Funding: This research received no external funding.

Data Availability Statement: Data is contained within the article.

Acknowledgments: Authors would like to express the sincere gratitude to the anonymous referees for their reviews, which resulted in significant improvements of the paper.

Conflicts of Interest: The authors declare no conflicts of interest.

References

1. Kress, R. *Linear Integral Equations*, 3rd ed.; Springer: New York, NY, USA, 2014.
2. Costabel, M.; Sayas, F.J. Time-dependent problems with the boundary integral equation method. In *Encyclopedia of Computational Mechanics*, 2nd ed.; John Wiley & Sons: New York, NY, USA, 2017. [CrossRef]
3. Lubich, C.; Schneider, R. Time discretization of parabolic boundary integral equations. *Numer. Math.* **1992**, *63*, 455–481. [CrossRef]
4. Chapko, R.; Kress, R. Rothe's method for the heat equation and boundary integral equations. *J. Integr. Equat. Appl.* **1997**, *9*, 47–69. [CrossRef]
5. Chapko, R.; Kress, R. On the numerical solution of initial boundary value problems by the Laguerre transformation and boundary integral equations. In *Integral and Integrodifferential Equations: Theory, Methods and Applications*; Series in Mathematical Analysis and Applications; Agarwal, R., O'Regan, D., Eds.; Gordon and Breach Science Publishers: Amsterdam, The Netherlands, 2000; Volume 2, pp. 55–69.
6. Chapko, R.; Johansson, B. Numerical solution of the Dirichlet initial boundary value problem for the heat equation in exterior 3-dimensional domains using integral equations. *J. Eng. Math.* **2017**, *103*, 23–37. [CrossRef]
7. Hohage, T.; Sayas, F. Numerical solution of a heat diffusion problem by boundary elements methods using the Laplace transform. *Numer. Math.* **2005**, *102*, 67–92. [CrossRef]
8. Chen, H.; Chen, C. Application of hybrid Laplace transform/finite-difference method to transient heat conduction problems. *Numer. Heat Transf.* **1988**, *14*, 343–356. [CrossRef]

9. Cai, X.D.; Costache, G. A Laplace domain finite element method (LDFEM) applied to diffusion and propagation problems in electrical engineering. *Int. J. Numer. Model. Electron. Netw. Devices Fields* **1994**, *7*, 419–432. [CrossRef]
10. Costabel, M. Developments in boundary element methods for time-dependent problems. In *Problems and Methods in Mathematical Physics*; Vieweg+Teubner Verlag: Wiesbaden, Germany, 1994; pp. 17–32. [CrossRef]
11. Brebbia, C.; Telles, J.; Wrobel, L. *Boundary Element Techniques: Theory and Applications in Engineering*; Springer: Berlin/Heidelberg, Germany, 2012.
12. Cohen, A.M. *Numerical Methods for Laplace Transform Inversion*; Series in Numerical Methods and Algorithms, Volume 5; Springer: New York, NY, USA, 2007.
13. López-Fernández, M.; Palencia, C. On the numerical inversion of the Laplace transform of certain holomorphic mappings. *Appl. Numer. Math.* **2004**, *51*, 289–303. [CrossRef]
14. Dingfelder, B.; Weideman, J.A.C. An improved Talbot method for numerical Laplace transform inversion. *Numer. Algorithms* **2015**, *68*, 167–183. [CrossRef]
15. Weideman, J.A.C.; Trefethen, L.N. Parabolic and hyperbolic contours for computing the Bromwich integral. *Math. Comput.* **2007**, *76*, 1341–1356. [CrossRef]
16. Talbot, A. The accurate numerical inversion of Laplace transforms. *IMA J. Appl. Math.* **1979**, *23*, 97–120. [CrossRef]
17. Kuhlman, K.L. Review of inverse Laplace transform algorithms for Laplace-space numerical approaches. *Numer. Algorithms* **2013**, *63*, 339–355. [CrossRef]
18. Davies, B.; Martin, B. Numerical inversion of the Laplace transform: A survey and comparison of methods. *J. Comput. Phys.* **1979**, *33*, 1–32. [CrossRef]
19. Davies, B. *Integral Transforms and Their Applications*; Texts in Applied Mathematics; Springer: New York, NY, USA, 2012.
20. Wienert, L. Die Numerische Approximation von Randintegraloperatoren für die Helmholtzgleichung im $\mathbb{R}^3$. Ph.D. Thesis, University of Göttingen, Göttingen, Germany, 1990.
21. Bellman, R.E.; Roth, R.S. *The Laplace Transform*; World Scientific: Singapore, 1984.
22. Weideman, J.A.C.; Fornberg, B. Fully numerical Laplace transform methods. *Numer. Algorithms* **2023**, *92*, 985–1006. [CrossRef]
23. Andersson, F. Algorithms for unequally spaced fast Laplace transforms. *Appl. Comput. Harmon. Anal.* **2013**, *35*, 419–432. [CrossRef]
24. Gustavsen, B.; Semlyen, A. Rational approximation of frequency domain responses by vector fitting. *IEEE Trans. Power Deliv.* **1999**, *14*, 1052–1061. [CrossRef]
25. Campos, R.G.; Díaz, F.M. Quadrature formulas for the Laplace and Mellin transforms. *BIT Numer. Math.* **2009**, *49*, 477–486. [CrossRef]
26. Churchill, R.V. *Operational Mathematics*, 3rd ed.; McGraw-Hill: New York, NY, USA, 1972.
27. Colton, D.; Kress, R. *Integral Equation Methods in Scattering Theory*; John Wiley & Sons: New York, NY, USA, 1983.
28. Abramowitz, M.; Stegun, I. *Handbook of Mathematical Functions with Formulas, Graphs, and Mathematical Tables*; National Bureau of Standards Applied Mathematics Series: Washington, DC, USA, 1972.